Talanta 213 (2020) 120815

Contents lists available at ScienceDirect

Talanta

journal homepage: www.elsevier.com/locate/talanta

Combining whispering gallery mode optofluidic microbubble resonator sensor with GR-5 DNAzyme for ultra-sensitive lead ion detection

Liang Fu[a], Qijing Lu[a,*], Xianlin Liu[a], Xiaogang Chen[a], Xiang Wu[b], Shusen Xie[a]

[a] Key Laboratory of Optoelectronic Science and Technology for Medicine of Ministry of Education, Provincial Key Laboratory for Photonics Technology, Fujian Normal University, Fuzhou, 350007, China

[b] Department of Optical Science and Engineering, Fudan University, Shanghai, 200433, China

ARTICLE INFO

Keywords:
Whispering gallery mode
Microbubble
Lead ion
GR-5 DNAzyme

ABSTRACT

Lead ions are deleterious pollutants that often reach drinking water, and can cause significant harm to humans (particularly children). An ultra-sensitive lead ion detection method using a whispering gallery mode (WGM) optofluidic microbubble resonator and the classic GR-5 DNAzyme is proposed in this paper. With the auxiliary piranha and Ploy-L-lysine solution, GR-5 DNAzyme was successfully modified on the inner wall of a microbubble. The mode field distribution of the microbubble was analysed, and the optofluidic sensor with thin wall exhibited a maximum bulk refractive index sensitivity of 265.2 nm/RIU. Lead ions at concentrations ranging from 0.1 pM to 100 pM were tested using the proposed WGM optofluidic sensor. The noise was decreased to 2.43 fM using the self-referenced differential method. Thus, a limit of approximately 15 fM was obtained for the detection of lead ions using the WGM optofluidic biosensor. Eight competing metal ions were also used to evaluate the selectivity of the proposed sensor, with results indicating that it has high selectivity for lead ions. Finally, the sensor performance is verified using real samples.

1. Introduction

Lead is one of the most toxic metals found in the natural environment, which has attracted attention because of its deleterious effects. Lead ions can enter the body via accumulation in the food chain. Even low concentrations of lead ions in food or drinking water can be harmful to human health. Reproductive, neurological, cardiovascular, and developmental disorders are fairly common symptoms of lead poisoning [1–3]. Children are especially vulnerable to lead ions [4]. The Environment Protection Agency (EPA) of the United States has ruled that the maximum concentration of lead ions in drinking water should not exceed 72 nM [3]. Rossi et al. showed that the concentration threshold for this pollutant should in fact be lower than 1 pM [5]. In order to reduce the impact of lead ions on human health, numerous efforts have been made in order to accurately detect concentrations of lead ions. Traditional instrumental analyses that have been used to investigate ion concentrations include atomic absorption/emission spectrometry [6], inductively coupled plasma mass spectrometry (ICP-MS) [7], x-ray fluorescence spectrometry (XRF) [8], anodic stripping voltammetry [8] and reversed-phase high-performance liquid chromatography coupled with UV–vis [9], among others. These methods are highly sensitive in terms of Pb^{2+} detection, and the detection limits of these methods are lower than the requirements of the EPA. However, most of these methods require expensive equipment and professional operatives [10]; hence, the rapid detection of lead ions is difficult to achieve in-situ. It is therefore important that a sensitive, selective, easily operated, and cheap platform is developed for better detection of poisonous lead ions.

In addition to methods that utilize instrumental analysis, chemical and biological sensors that are based on the use of DNA enzymes have been studied extensively in recent years, because of both the high catalytic turnover that allows the amplification of a signal and the lower vulnerability to interference from background noise. The first DNAzyme that used Pb^{2+} as a cofactor was 8–17 DNAzyme, which was discovered in 1994 [11]. The next DNAzyme that was developed, GR-5 DNAzyme, has a similar structure and properties to 8–17 DNAzyme; however, it has better selectivity for lead ions over other competing metal ions [10,12]. As a whispering gallery mode (WGM) microresonator sensor, it has a high quality factor (Q) and an ultra-small mode volume (V) [13,14], and has been used for the detection of nanoparticles [15], single molecules [16], DNA [17], proteins [18] and other particulate matter [19,20]. Panich et al. [21] used the WGM microsphere resonator sensor with glutathione to detect lead ions; however, the bulk refractive index sensitivity of the microsphere is far

* Corresponding author.
E-mail address: qjlu@fjnu.edu.cn (Q. Lu).

https://doi.org/10.1016/j.talanta.2020.120815
Received 20 August 2019; Received in revised form 6 February 2020; Accepted 8 February 2020
Available online 10 February 2020
0039-9140/

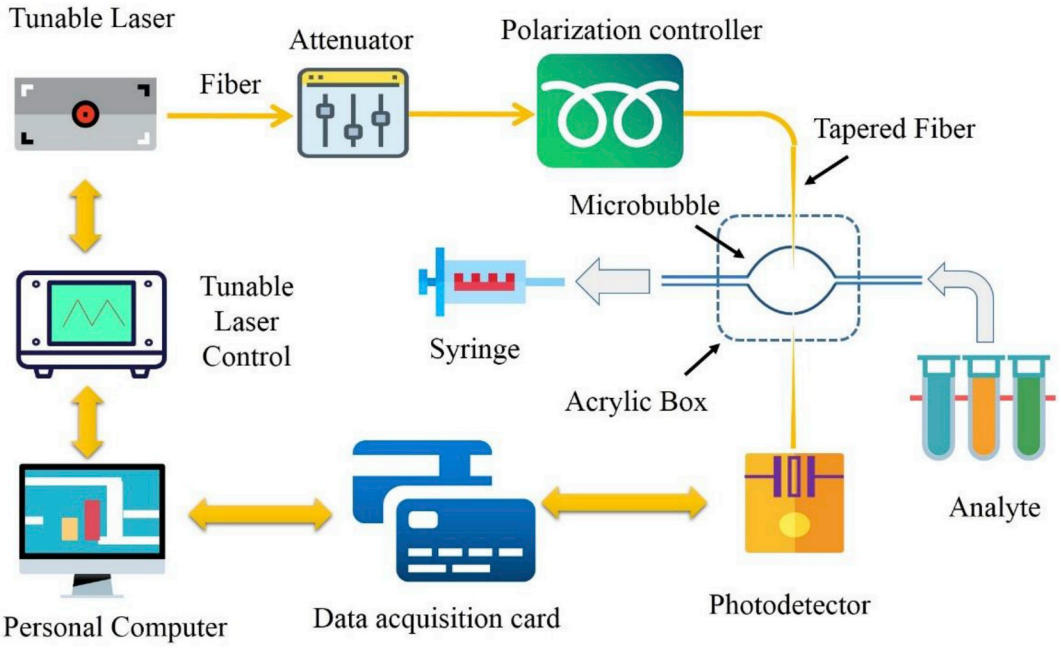

Fig. 1. The schematic of the WGM optofluidic sensing setup.

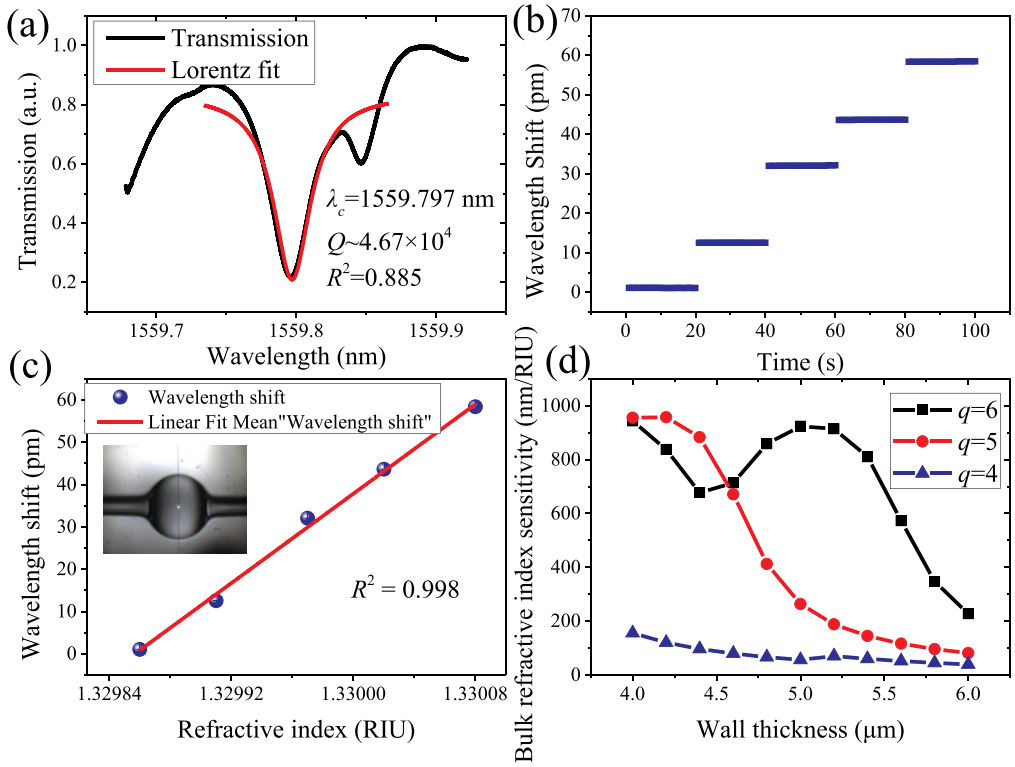

Fig. 2. (a) The WGM used in the bulk refractive index sensitivity characterization. (b) Measured resonance wavelengths of the WGM as a function of the RI of the alcoholic aqueous solution. (c) The linear result of fitting the measured data. The coupling of the microbubble and tapered fiber as illustrated in the insert. (d) The results of the analysis using the Mie theory for modes q = 4, 5, 6.

less than that of the microbubble. The flow cell that was used in this experiment also rendered the sensor less practical. WGM sensors that are based on optofluidic microbubble resonators have natural microchannels, and are therefore particularly suitable for the detection of liquid analytes [22].

In this study, we propose a WGM biosensor based on an optofluidic microbubble resonator (MBR) together with the GR-5 DNAzyme for the ultra-sensitive and highly-selective detection of lead ions. Through the continuous corrosion with the hydrofluoric (HF) acid, an optofluidic MBR with ultrathin walls can be obtained with a bulk refractive index sensitivity that reaches as high as 265.2 nm/RIU. The ultra-sensitive detection of lead ions in deionized (DI) water was achieved by attaching DNA to the inner wall of the microbubble resonator. Experimental results indicated that the detection limit of the proposed sensor is

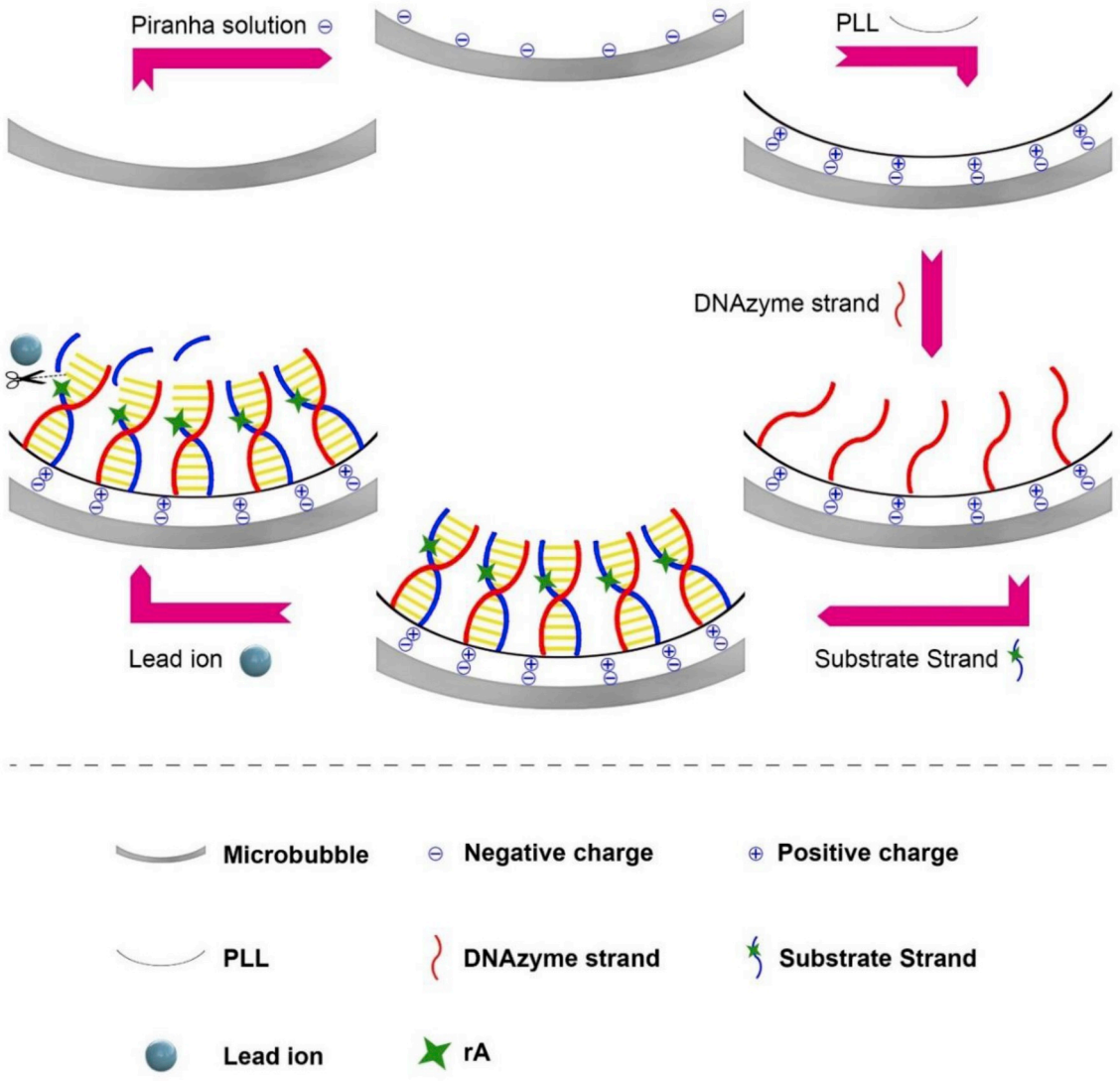

Fig. 3. The complete process of the surface functionalization. The piranha solution, PLL solution, DNAzyme strands, and substrate strands are pumped into to microbubble in sequence. Notes of the items used in the figure are below the dotted line.

approximately 15 fM, which is 3 orders lower than that of the microsphere resonator [21]. The WGM optofluidic biosensor also exhibits good selectivity over competing metal ions. The proposed sensor was finally used to detect lead ions in a real sample. This WGM optofluidic sensor for the detection of Pb^{2+} has potential application in environmental monitoring and food safety analysis, among several other possibilities.

2. Experimental section

The two oligonucleotides used in this experiment were purchased from Sangon Biotech Co., Ltd (Shanghai, China); the sequence of the DNAzyme used is 5′-ACAGACATCATCTCTGA AGTAGCGCCGCCGTAT AGGAG-3′ and the substrate sequence is 5′-CTCACTATrAGGAAGA GATGATGTCTGT-3'. These two specific oligonucleotides were chosen following the research by Yildirim et al. [23]. The Ploy-L-lysine solution (PLL, 0.1% w/v in water, with a molecular weight of 150,000–300, 000) was purchased from Sigma (Shanghai, China). Except for the 0.05 M lead nitrate standard titration, which was purchased from Aladdin (Shanghai, China), all metal salts used in the selectivity test including NaCl, $CaCl_2$, $ZnCl_2$, KCl, $CuCl_2$, $FeCl_3$, $FeCl_2$, and $MnCl_2$, were obtained from Sinopharm Chemical Reagent Co., Ltd (Shanghai, China). All the metal salts were dissolved in DI water. The concentrated sulfuric acid and hydrogen peroxide used to prepare the piranha solution (a mixture of 7 vol of concentrated H_2SO_4 with 3 vol of 30% H_2O_2) also come from the Sinopharm Chemical Reagents. The phosphate buffer solution (PBS, 0.01 M Na_2HPO_4, pH = 7.2–7.4) was purchased from Solarbio (Beijing, China).

The detailed process used for the fabrication of the microbubble can be found in previous work [24]. First, a fusion splicer was used to melt one end of the capillary at a high temperature in order to seal it. The other end of the capillary was then connected to a syringe with a Teflon tube. Finally, air was compressed into the capillary tube while the middle part of the capillary tube was heated via electrode discharge. The heated part expands under adequate internal pressure, leading to the fabrication of a microbubble. Both ends of the capillary containing the microbubble were then connected to the Teflon tube, forming the fluidic channel into which liquid analytes can flow.

The initial thickness of the wall of the capillary tube measured using the fluorescence microscope (Olympus, BX61W1) was 25 μm. The thickness was reduced to 15 μm because of the conservation of volume after the fabrication of the microbubble. The mode field distribution of the microbubble cavity was analysed using the Mie scattering theory. The results of the calculation indicate that most of the mode field will

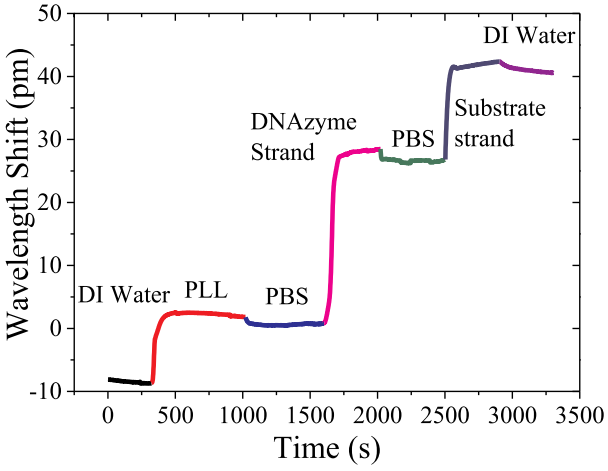

Fig. 4. The resonance wavelength shifts as a function of time during the process of surface functionalization. The three curves (red, magenta, and navy) that illustrate a red shift in the wavelength indicate that the PLL, the DNAzyme strands, and the substrate strands have been successfully attached to the inner wall of microcavity in sequence. The three other curves (blue, navy, and violet lines) demonstrate a blue shift in the wavelength, indicating the sequential removal of superfluous modifier. (For interpretation of the references to colour in this figure legend, the reader is referred to the Web version of this article.)

be distributed in the liquid core when the wall of the microbubble resonator is thin. Hydrofluoric acid was therefore used to corrode the wall of the microbubble resonator. After 90 min of etching with 10% HF acid, a thickness of approximately 6 μm was achieved in the wall of the microbubble resonator. The 4% HF acid was then used to further corrode the microbubble resonator. Lower concentrations of HF acid were used for two purposes; the wall of the microbubble resonator is already highly thin, and using low concentrations of HF acid slows the speed of corrosion, ensuring that the wall of the microbubble resonator is not perforated. This slow corrosion is equivalent to the chemical polishing of the inner wall of the microbubble resonator. This means that the *Q* value of the microbubble resonator is still high when the inner wall is thin. A final thickness of approximately 5 μm was obtained.

The schematic of the experimental setup is shown in Fig. 1. Light from a tunable laser (Toptica Photonics, CTL 1550) is coupled with the microbubble resonator through the tapered fiber and used for exciting the WGM resonance. The output port of the tapered fiber is connected to the photo detector (Thorlabs, PDA10CF-EC). The voltage signals formed on the photo detector are all collected by the data acquisition card (National Instruments, X SERIES DAQ 781048–01) in real time with a collection interval of 1 s. The other port of the data acquisition card inputs a triangular wave tuning signal to the laser. The data acquisition and laser control are carried out using customized LabVIEW software. All liquid flowing through the microbubble is controlled with a syringe micropump (Harvard Apparatus, Pump 11 Pico Plus Elite) at 10 μL/min. In order to reduce the impact of environmental changes on the experiment, the coupling of the microbubble and the tapered fiber is sealed within a transparent acrylic box.

The general principle of the WGM sensing device is based on the shift in the wavelength of the WGM resonance and can be described as follows. The sensor is initially in a stable state, and the resonant wavelength in the microcavity is at a fixed value. The resonant wavelength of the microcavity can be described using [25] as

$$m\lambda_c = 2\pi R n_{eff}, \tag{1}$$

where m is the azimuthal quantum number, λ_c is the resonance wavelength, R is the radius of the microbubble cavity, and n_{eff} denotes the effective refractive index of the WGM. The resonant wavelength

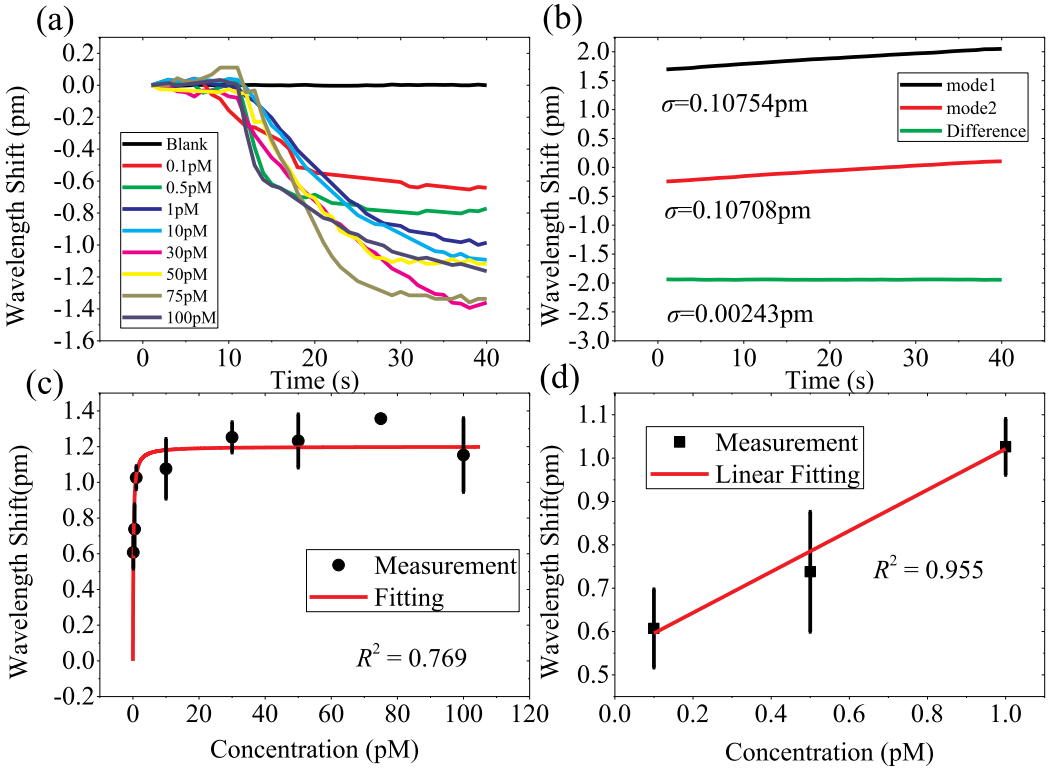

Fig. 5. (a) The WGM resonance wavelength as a function of time when the lead ion solution enters the microbubble at different concentrations. (b) The self-referenced differential method for two different modes and the differential result. (c) Measurement data and calibration curve. (d) Linear fitting results for low concentrations.

Table 1
The comparison of the LOD of Our Work and previous lead ion sensors.

Method	Strategy	Linear range	LOD	Reference
Microfiber Resonator	Black phosphorus functionalized microfiber coil resonator	Not mentioned	0.14 nM	[29]
Strip biosensor	Graphene oxide-assisted Au nanoparticle strip biosensor based on GR-5 DNAzyme	0.01–100 μM	0.05 nM	[36]
Fluorescence	DNAzyme based biosensor on a Portable Optic Fiber	2–75 nM	1.03 nM	[23]
Colorimetry	Colorimetric aptasensor using polyethyleneimine and AuNPs	0–10 nM	702 pM	[37]
Colorimetry	Colorimetric sensor based on DNAzyme	0.1–1 mM	100 pM	[38]
WGM resonator	WGM microsphere using GSH − Au NPs	2.4–48.26 nM	0.05 nM	[21]
optofluidic WGM resonator	WGM microbubble using GR-5 DNAzyme	0.1–1 pM	15 fM	This study

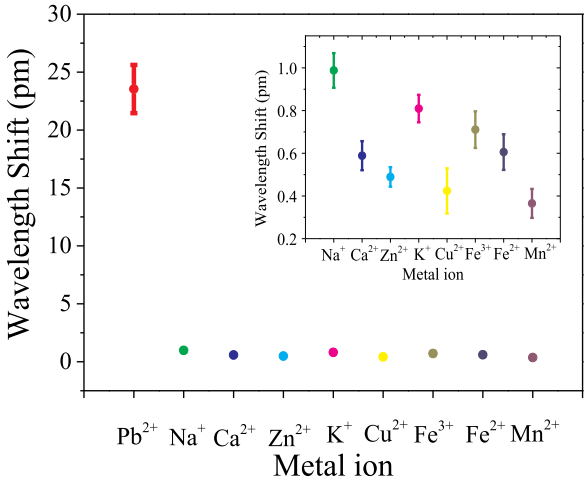

Fig. 6. The wavelength shifts for lead ions and eight competing metal ions. The inset shows the signals of the eight competing metal ions with the associated error bars.

depends only on the effective refractive index of a specific microbubble. When the analyte enters the sensing area (microcavity), the effective refractive index of the WGM changes, which leads to a change in the resonant wavelength of the microcavity. The resonant wavelength of the microcavity is initially fixed in the proposed lead ion sensor. The DNA that is attached onto the inner wall of the microcavity is cut when the lead ions enter the microcavity. The effective refractive index and resonant wavelength of the WGM is gradually reduced until the reaction reaches a balanced state, and the resonant wavelength of the microcavity then returns to a stable state.

3. Result and discussion

The bulk refractive index sensitivity of the microbubble resonator was characterized before the surface functionalization was initiated, using an alcoholic aqueous solution with a refractive index gradient of 0.00005. The bulk refractive index of the microbubble was obtained by calculating the slope of the resonant wavelength shift versus the refractive index change. The relationship between Q and resonance wavelength can be written [26] as

$$Q = \frac{\lambda_c}{\Delta\lambda}, \tag{2}$$

where λ_c is the resonance wavelength and $\Delta\lambda$ denotes the full width at half maximum (FWHM) of the WGM, respectively. The transmission of the WGM (black curve) and the Lorentz fit result (red curve) is shown in Fig. 2(a). The resonance wavelength and the Q of the WGM are approximately 1559.797 nm and 4.67×10^4, respectively. The change in the resonant wavelength with the refractive index is shown in Fig. 2(b). The expression for the sensitivity of the sensor is as follows [27]:

$$S = \frac{\delta[output]}{\delta[input]}, \tag{3}$$

where S is the bulk refractive index sensitivity, δ[output] is the change in the wavelength shift of the WGM, and $\delta[input]$ denotes the change in refractive index. The linear fitting of the refractive index and resonance wavelength according to Eq. (3) is shown in Fig. 2(c), and a result of approximately 265.2 nm/RIU was calculated in this study, which is appropriate for ultra-sensitive detection. The Mie theory was utilized in order to analyse the mode used for sensing. The sensitivity of the radial modes (q = 4, 5, 6) with different wall thicknesses is shown in Fig. 2(d). As mentioned previously, the thickness of the microbubble wall is approximately 5 μm, and the results indicate that the mode tested corresponds to the radial fifth order mode (q = 5).

The general surface functionalization procedures used were based on those developed by Liu et al. [28]. The complete functionalization process is shown in Fig. 3. The purpose of the functionalization is to fix the GR-5 DNAzyme onto the inner wall of the microbubble resonator. The GR-5 DNAzyme cannot effectively bind to the silica wall alone, meaning that pre-treatment of the inner wall is necessary. The piranha and PLL solutions are used to achieve this. PLL has a positive charge while single strands of DNA have a negative charge; the PLL can therefore be used to absorb single strand DNA. The piranha solution was allowed to flow through the microchannel for 1 h prior to the addition of the PLL. The microbubble was then washed in the DI water for 30 min, resulting in a negatively charged silica surface. The PLL

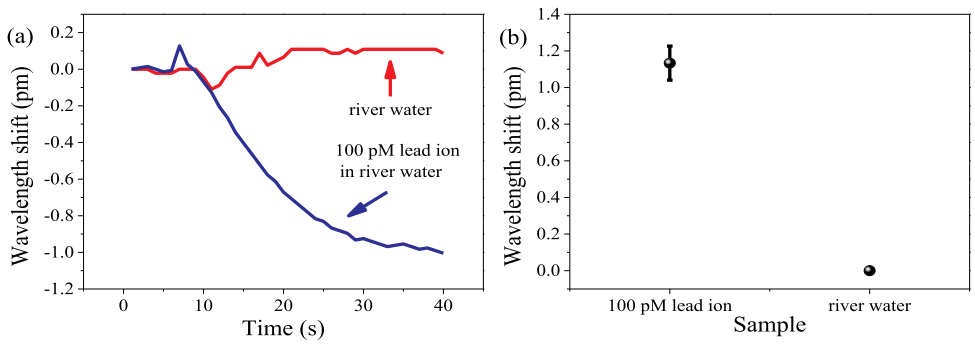

Fig. 7. Experimental results for the sensors in real samples. (a) Curve describing the change in the resonance wavelength of the river water (red line) and the 100 pM Pb^{2+} river water (blue line). (b) The average signals with error bars generated by 100 pM lead ions and river water. (For interpretation of the references to colour in this figure legend, the reader is referred to the Web version of this article.)

solution was then pumped into the microbubble for 1 h, after which the microbubble was washed with PBS in order to remove the redundant PLL, leaving a monolayer of PLL om the wall of the microbubble. The 1 μM DNAzyme strands were then1 dissolved in the PBS and injected into the microchannel for 1 h, from which the DNAzyme strands were attached to the wall. Finally, the 1 μM substrate strands were also dissolved in the PBS and pumped into the microbubble for 1 h. Hybrids of the substrate and DNAzyme strands were then absorbed onto the PLL, and the GR-5 DNAzyme was successfully functionalized onto the inner wall of microbubble. The changes to the resonance wavelength of the WGM were recorded during the process of functionalization, as shown in Fig. 4.

DI water was pumped into the microbubble after completion of the surface functionalization, in order to find the best WGM for sensing, followed by the lead ion solution. Experiments were carried out using eight different concentrations of lead ions ranging from 0.1 pM to 100 pM. The lead ion solutions were diluted using a 0.05 M lead nitrate standard titration solution. All transmission spectra were recorded and changes in the resonance wavelength were analysed via Lorentz Fitting that was conducted with customized MATLAB code. Fig. 5(a) shows the change in the WGM resonance wavelength as a function of time. It should be emphasized that the response speed of the sensor is high, and the time taken between the first ion entering the microcavity and the end of the reaction is no more than 20 s. This is significantly faster than traditional optical fiber sensors, which take approximately 50 s [29]. As can be seen from Fig. 5(a) the signal generated by the sensor varies under different concentrations. However, the trend in the changes to the resonance wavelength is the same, and the general process can be described as follows. Before lead ions are pumped into the modified microbubble, the resonance wavelength is nearly constant. After the motion of the lead ion solution through the microbubble, the resonance wavelength shifts gradually towards the blue end of the spectrum, after which it stabilizes. This is because the lead ions cleave the substrate strands of the GR-5 DNAzyme modified onto the inner walls of microbubble, and chemical equilibrium is attained between the lead ions and GR-5 DNAzyme. The variation in the resonant wavelength caused by the different concentrations of lead was then changed into the absolute value. The signal generated by the different concentrations of lead ions is portrayed using black dots in Fig. 5(c). The calibration curve (red line) for the detection of the lead ions in the DI water in Fig. 5(c) can be fitted via the Michaelis–Menten model according to the following equation [30]:

$$\delta\lambda = \frac{\delta\lambda_{\max}[Pb^{2+}]}{K_d + [Pb^{2+}]}, \tag{4}$$

where $\delta\lambda$ is the measured shift in the resonance wavelength, $\delta\lambda_{\max}$ is the maximum shift in wavelength obtained in the experiment, $[Pb^{2+}]$ is the lead ion concentration, and the K_d is the dissociation constant. A value of approximately 0.16 pM was obtained for K_d and 1.2 pm for $\delta\lambda_{\max}$ via the fitting process. The value of K_d is much smaller than that obtained using the Hill-1 function [31], from which a dissociation constant of 217 nM was obtained. This effect could be attributed to the different binding ability of the GR-5 DNAzyme with the Hill-1 function [32]. Fig. 5(d) illustrates the linear fitting between the lead ion concentration and the shift in wavelength at low concentrations, from which a sensitivity of 0.4726 pm/pM was obtained. The linear fitting was carried out according to Eq. (3), in which *δ[output]* describes the change in the wavelength shift of WGM, and *δ[input]* denotes the change in the concentration of lead ions.

After studying the sensitivity of the sensor, another important parameter was also calculated; the limit of detection (LOD). The LOD is determined by blank signal standard deviation $\sigma[\delta\lambda]$ and can be expressed as follows [33,34]:

$$LOD = \frac{R}{S} = \frac{3\sigma[\delta\lambda]}{S}, \tag{5}$$

where S is the sensitivity of the sensor and R is the resolution of the sensor. R is equal to the triple blank signal standard deviation $\sigma[\delta\lambda]$. When the sensitivity is determined, the detection limit can only be reduced by reducing the noise. The noise generated by environmental effects (such as mechanical vibration or temperature) and the instability in the laser are almost the same in a specific microbubble. This means that the change in the resonance wavelength of the two modes are almost the same. If the curve demonstrating a change in the wavelength in mode 1 is subtracted from that of mode 2, the noise can be almost eliminated. Zhang et al. [35] proposed a self-referenced differential sensing method to reduce noise based on this theory, where the noise from vibration was limited by the noise from the laser power instability (σ = 2 fm). The same method was applied in this study in order to reduce the noise. After processing the noise data, including mode 1 (black line) and mode 2 (red line) via the self-referenced differential method, the noise was reduced to 2.43 fm, as seen in Fig. 5(b). Finally, a LOD of nearly 15 fM was observed in the optofluidic WGM biosensor when carrying out lead ion detection. The LOD of the sensor is far lower than the requirements of the EPA. The setup in this study, which was based on a WGM optofluidic microbubble biosensor, has two advantages when compared to Panich et al. [21], who used a WGM microsphere and glutathione for lead ion detection. One is the presence of natural microfluidic channels without the need for any additional microfluidic cells, making it more suitable for detection using fluids. The other is the higher bulk refractive index sensitivity, which is due to the adjustable wall thickness; this means that it can respond to lead ion solutions at lower concentrations. Thus the LOD of our microbubble sensor is three orders of magnitude lower than that of the microsphere sensor. We also compared the LOD and the linear range of the proposed sensor with those previously reported (Table 1). The LOD of our sensor is significantly lower than that obtained using these methods.

To evaluate the selectivity of the proposed WGM biosensor, eight competing metal ions (Na^+, Ca^{2+}, Zn^{2+}, K^+, Cu^{2+}, Fe^{3+}, Fe^{2+}, and Mn^{2+}) were tested under the same experimental conditions as that used for Pb^{2+}. The results of this test are shown in Fig. 6, with the inset demonstrating the signal and error bars of the eight other metal ions. A relatively high concentration of these ions was chosen in order to adequately study the response of the sensor to other non-specific metal ions. A concentration of > 1 μM of metal ions was used in the selectivity test, including the lead ions. The results of this experiment indicate a shift in wavelength of > 20 pm for 1 μM Pb^{2+}. However, the maximum wavelength obtained for the eight competing metal ions was approximately 1.1 pm, or approximately one-twentieth of the signal obtained for Pb^{2+} under the same experimental conditions. The WGM wall sensor therefore has better selectivity compared to the optical fiber sensor [39] and the surface enhanced Raman sensor [40]. These experimental results mean that the WGM biosensor has higher selectivity for lead ions than other metal ions.

After verifying the selectivity of the sensor, identical investigations were carried out using real samples. River water was obtained from the water source protection area of Minjiang River (Fuzhou, China). In order to obtain clear and transparent analytical samples, the river water was centrifuged and filtered to remove any suspended solids and impurities. Following the centrifugation and filtration, the standard lead nitrate solution was diluted with river water to obtain a lead nitrate solution with a concentration of 100 pM. The sensor was then used to test both the pure river water and the 100 pM Pb^{2+} solution three times, the results of which are shown in Fig. 7(a). It can be seen from the figure that the curve describing the change in wavelength caused by the presence of lead ions is almost the same in both DI water (Fig. 5(a)) and river water with a Pb^{2+} concentration of 100 pM. Observations showed that the resonance wavelength is initially stable and unchanging. When the lead ions enter the sensor, the resonance wavelength gradually shifts to blue. After the reaction between the lead and the DNA reaches equilibrium, the resonance wavelength is stable and remains unchanged. However, little signal was produced when river

water was used. Some small step-by-step changes were observed in the resonance wavelength as the water enters the sensor. It is worth noting that this signal is not the generated by the sensor, the little change seen in the resonance wavelength is due to the tiny difference in the refractive index between the river water and the DI water. Fig. 7(b) shows the average and the error bar of the three signals generated by the 100 pM lead ions and the river water.

4. Conclusion

In this paper, a label-free method for ultra-sensitive detection of lead ions was demonstrated using a WGM microbubble resonator and GR-5 DNAzyme. The GR-5 DNAzyme was successfully modified on the inner wall of the microbubble with the aid of piranha solution and PLL solution. A bulk refractive index sensitivity of 265.2 nm/RIU was obtained for the microbubble resonator. The LOD of the WGM biosensor was decreased to 15 fM by using a self-referenced differential for suppression of the noise. The selectivity of the sensor is higher to lead ions than eight competing metal ions. In addition, the practical application of the sensor is confirmed by the results from tests using real samples. The proposed sensor is low cost, simple to operate, and has fast testing speed. The proposed WGM biosensor for lead ion detection therefore has potential value for application value in monitoring drinking water, and food. For detecting lead ions in solid samples such as food, these samples should be crushed, centrifuged and filtered to obtain a clear solution. It is worth pointing out that other competing metal ions in real samples could interfere with the determination accuracy. The selectivity should be further improved as compared with commercial instruments such as atomic emission spectrometry. It is expected that the sensing device can also be further optimized in future studies in order to obtain a lower detection limit. A feasible method for achieving this could be via the use of a low refractive index ultraviolet glue to completely cover the coupling of the microcavity and taper fiber, cured with ultraviolet light to obtain an encapsulated sensor device. This would improve the robustness of the system and reduce the noise, while allowing portability; hence, the sensor device could be used for in-situ detection of lead ions. An alternative means could be the adoption of Au nanoparticles in order to obtain a plasmonic mode, which also has the potential to improve the performance of the sensor and decrease the detection limit.

5. Notes

The authors declare no competing financial interest.

Declaration of competing interest

We declare that we do not have any commercial or associative interest that represents a conflict of interest in connection with the work submitted.

Acknowledgements

This work was supported the National Natural Science Foundation of China under Grants Nos. 61705039; National Key Basic Research Program of China (973 project) under Grant No. 2015CB352006; China Postdoctoral Science Foundation (2019T120553, 2017M610389); Fujian Provincial Program for Distinguished Young Scientists in University; Fujian Provincial Key Project of Natural Science Foundation for Young Scientists in University (JZ160423); Program for Changjiang Scholars and Innovative Research Team in University under Grant No. IRT_15R10; Special Funds of the Central Government Guiding Local Science and Technology Development (2017L3009).

References

[1] S. Basak, N. Nandi, S. Paul, I.W. Hamley, A. Banerjee, Chem. Commun. 53 (2017) 5910.
[2] A. Carocci, A. Catalano, G. Lauria, M.S. Sinicropi, G. Genchi, Rev. Environ. Contam. Toxicol. 238 (2015).
[3] L. Wang, Y. Wen, L. Li, X. Yang, G. Liu, Biosens. Bioelectron. 115 (2018).
[4] Y. Ge, L. Qin, Z. Li, Mater. Des. 95 (2016) 141–147.
[5] E. Rossi, Clin. Biochem. Rev. 29 (2008) 63–70.
[6] X. Wang, C. Niu, L. Guo, L. Hu, S. Wu, G. Zeng, F. Li, J. Fluoresc. 27 (2017) 643–649.
[7] T. Shih, C. Hsieh, Y. Luo, Y. Su, P. Chen, Y. Chuang, Y. Sun, Anal. Chim. Acta 916 (2016) 24–32.
[8] H. Lin, M. Li, D. Mihailovi, Electrochim. Acta 154 (2015) 184–189.
[9] M. Thirumalai, S.N. Kumar, D. Prabhakaran, N. Sivaraman, M.A. Maheswari, J. Chromatogr., A 1569 (2018) 62–69.
[10] F. Wang, Z. Wu, Y. Lu, J. Wang, J. Jiang, R. Yu, Anal. Biochem. 405 (2010) 168–173.
[11] R.R. Breaker, G.F. Joyce, Chem. Biol. 1 (1994) 223.
[12] L. Tian, F. Kimberly, L. Yi, Chem. Commun. 46 (2010) 3896–3898.
[13] K.J. Vahala, Nature 424 (2003) 839.
[14] M.R. Foreman, J.D. Swaim, F. Vollmer, Adv. Optic Photon 7 (2015) 168–240.
[15] W. Chen, J. Zhang, B. Peng, Ş.K. Özdemir, X. Fan, L. Yang, Photon. Res. 6 (2018) A23–A30.
[16] T. Jollans, M.D. Baaske, M. Orrit, J. Phys. Chem. C 123 (2019) 14107–14117.
[17] P. Toren, E. Ozgur, M. Bayindir, Anal. Chem. 87 (2015) 10920–10926.
[18] K.A. Wilson, C.A. Finch, P. Anderson, F. Vollmer, J.J. Hickman, Biomaterials 38 (2015) 86–96.
[19] E. Kim, M.D. Baaske, F. Vollmer, Lab Chip 17 (2017) 1190–1205.
[20] M.R. Foreman, J.D. Swaim, F. Vollmer, Adv. Optic Photon 7 (2015) 168–240.
[21] P. Sirirat, K.A. Wilson, N. Philippa, C.K. Wood, A. Tim, J.B. Edel, Anal. Chem. 86 (2014) 6299.
[22] I.M. White, O. Hesam, F. Xudong, Opt. Lett. 31 (2006) 1319–1321.
[23] N. Yildirim, F. Long, M. He, C. Gao, H.C. Shi, A.Z. Gu, Talanta 129 (2014) 617–622.
[24] Q. Lu, S. Liu, X. Wu, L. Liu, L. Xu, Opt. Lett. 41 (2016) 1736.
[25] Y. Zhi, X. Yu, Q. Gong, L. Yang, Y. Xiao, Adv. Mater. 29 (2017) 1604920.
[26] G. Lin, A. Coillet, Y.K. Chembo, Adv. Optic Photon 9 (2017) 828–890.
[27] Z. Guo, Q. Lu, C. Zhu, B. Wang, Y. Zhou, X. Wu, Optic Express 27 (2019) 12424–12435.
[28] Q. Liu, S. Chen, W. Peng, Y. Liu, Optic Express 23 (2015) 20686–20695.
[29] Y. Yin, S. Li, S. Wang, S. Jia, J. Ren, G. Farrell, E. Lewis, P. Wang, Photon. Res. 7 (2019) 622–629.
[30] J.D. Suter, I.M. White, H. Zhu, H. Shi, C.W. Caldwell, X. Fan, Biosens. Bioelectron. 23 (2008) 1003–1009.
[31] C. Dolain, H. Jiang, J.M. Léger, P. Guionneau, I. Huc, J. Am. Chem. Soc. 127 (2005) 12943.
[32] L. Marbella, B. Serli-Mitasev, P. Basu, Angew. Chem. 121 (2009) 4056–4058.
[33] H.P. Loock, P.D. Wentzell, Sensor. Actuator. B Chem. 173 (2012) 157–163.
[34] I.M. White, X. Fan, Optic Express 16 (2008) 1020–1028.
[35] X. Zhang, L. Liu, X. Lei, Appl. Phys. Lett. 104 (2014) 22242.
[36] H.B. Wang, L.H. Ma, B.Y. Fang, Y.D. Zhao, X.B. Hu, Colloids Surf., B 169 (2018) 305–312.
[37] S.M. Taghdisi, N.M. Danesh, P. Lavaee, M. Ramezani, K. Abnous, Environ. Toxicol. Pharmacol. 39 (2015) 1206–1211.
[38] C. Li, L. Wei, X. Liu, L. Lei, G. Li, Anal. Chim. Acta 831 (2014) 60–64.
[39] H. Yuan, W. Ji, S. Chu, Q. Liu, S. Qian, J. Guang, J. Wang, X. Han, J.-F. Masson, W. Peng, ACS Sens. 4 (2019) 704–710.
[40] Y. Shi, H. Wang, X. Jiang, B. Sun, B. Song, Y. Su, Y. He, Anal. Chem. 88 (2016) 3723–3729.